**This document is downloaded from DR-NTU (https://dr.ntu.edu.sg)
Nanyang Technological University, Singapore.**

Photo detection and modulation from 1,550 to 2,000 nm realized by GeSn/Ge multiple-quantum-well photodiode on 300-mm Si substrate

Zhou, Hao; Xu, Shengqiang; Wu, Shaoteng; Huang, Yi-Chiau; Zhao, Peng; Tong, Jinchao; Son, Bongkwon; Guo, Xin; Zhang, Dao Hua; Gong, Xiao; Tan, Chuan Seng

2020

Zhou, H., Xu, S., Wu, S., Huang, Y.-C., Zhao, P., Tong, J., ... Tan, C. S. (2020). Photo detection and modulation from 1,550 to 2,000 nm realized by GeSn/Ge multiple-quantum-well photodiode on 300-mm Si substrate. Optics Express, 28(23), 34772-34786. doi:10.1364/OE.409944

https://hdl.handle.net/10356/144386

https://doi.org/10.1364/OE.409944

© 2020 Optical Society of America under the terms of the OSA Open Access Publishing Agreement.

Downloaded on 13 Mar 2024 16:24:28 SGT

Research Article | Vol. 28, No. 23 / 9 November 2020 / Optics Express 34772
Optics EXPRESS

Photo detection and modulation from 1,550 to 2,000 nm realized by a GeSn/Ge multiple-quantum-well photodiode on a 300-mm Si substrate

HAO ZHOU,[1] SHENGQIANG XU,[2] SHAOTENG WU,[1] YI-CHIAU HUANG,[3] PENG ZHAO,[1] JINCHAO TONG,[1] BONGKOWN SON,[1] XIN GUO,[1] DAOHUA ZHANG,[1] XIAO GONG,[2] AND CHUAN SENG TAN[1,*]

[1]*School of Electrical and Electronic Engineering, Nanyang Technological University, 639798, Singapore*
[2]*Department of Electrical and Computer Engineering, National University of Singapore, 117576, Singapore*
[3]*Applied Materials Inc., Sunnyvale, CA 95054-3299, USA*
[*]*tancs@ntu.edu.sg*

Abstract: A GeSn/Ge multiple-quantum-well (MQW) *p-i-n* photodiode structure was proposed for simultaneously realizing high detectivity photo detection with low dark current and effective optical modulation based on the quantum confined Stark (QCSE) effect. The MQW stacks were grown on a 300-mm Ge-buffered Si substrate using reduced pressure chemical vapor deposition (RPCVD). GeSn/Ge MQW *p-i-n* photodiodes with varying mesa diameters were fabricated and characterized. An ultralow dark current density of 16.3 mA/cm^2 at -1 V was achieved as expected due to the low threading dislocation density (TDD) in pseudomorphic GeSn layer. Owing to the ultralow dark current density and high responsivity of 0.307 A/W, a high specific detectivity of 1.37×10^{10} cm·Hz$^{1/2}$/W was accomplished at 1,550 nm, which is comparable with commercial Ge and extended-InGaAs photodetectors. Meanwhile, the bias voltage-dependent photo response was investigated from 1,700 to 2,200 nm. The extracted effective absorption coefficient of GeSn/Ge MQW shows a QCSE behavior with electric field-dependent exciton peaks from 0.688 to 0.690 eV. An absorption ratio of 1.81 under -2 V was achieved at 2 μm, which shows early promise for effective optical modulation. The high frequency response was calculated theoretically, and the predicted 3-dB bandwidth for the photodiode with a mesa diameter of 30 μm could reach 12 GHz at -2 V.

© 2020 Optical Society of America under the terms of the OSA Open Access Publishing Agreement

1. Introduction

Ge photodetectors are widely used in the state-of-art silicon photonics since the direct bandgap of Ge is ~0.8 eV which exactly corresponds to a pivotal telecommunication band: C-band. The incorporation of another group IV material Sn is known to reduce the bandgap of Ge and the detection range of GeSn photodetectors with a small Sn fraction can cover all telecommunication bands from O-band to U-band (from 1,260 to 1,675 nm) [1–3]. Incorporating higher Sn concentration into Ge can even push the upper limit to longer wavelength and make it capable of photo detection at 2 μm [4]. Over the past decades, 2 μm band has received increasing interests due to its potential as a new communication window with advancement in hollow-core photonic-bandgap fibers (HC-PBGFs) and thulium-doped fiber amplifiers (TDFAs) [5–10]. GeSn-based photodetectors with enhanced and extended detectivity beyond 2 μm have been demonstrated [11–15]. In addition, optical modulation on the basis of Franz-Keldysh effect and lasing operation based on tuned direct bandgap in bulk GeSn have also been substantiated experimentally [16–21]. Therefore, GeSn has the potential to offer a monolithic integration

#409944 https://doi.org/10.1364/OE.409944
Journal © 2020 Received 10 Sep 2020; revised 21 Oct 2020; accepted 22 Oct 2020; published 2 Nov 2020

Optics EXPRESS

methodology for the entire suit of active photonics devices including laser, modulator, and photodetectors.

GeSn photodetectors suffer from higher dark current which degrades their detectivity compared with commercial Ge photodetectors. Due the lattice mismatch, GeSn with higher Sn fraction directly grown on Ge-buffered Si substrate is afflicted with higher threading dislocation density (TDD). The misfit dislocations not only act as generation/recombination centers for Shockley-Read-Hall (SRH) leakage current, but also offer energy states in the bandgap for trap-assisted tunneling (TAT) leakage current [22]. Taking the well-established knowledge from III-V quantum structures, GeSn/Ge MQW structure using pseudomorphic GeSn as well region is able to decrease the TDD significantly by avoiding strain relaxation. Moreover, MQW structure provides strong confinement for excitons at room temperature and the corresponding QCSE effect has been widely used for high speed and low power dissipation modulator. Although strong QCSE effect has been reported in Ge/SiGe MQW [23,24], it remains a mystery in GeSn/Ge MQW system.

In this work, $Ge_{0.92}Sn_{0.08}$/Ge MQW *p-i-n* photodiodes were fabricated and characterized. For the photodiode with mesa diameter of 250 μm, an ultralow dark current density of 16.3 mA/cm^2 at -1 V was achieved due to the pseudomorphic GeSn/Ge MQW design. The photo detection performance of the photodiode was examined from 1,550 to 2,000 nm. The fabricated *p-i-n* photodiode shows a high-efficiency optical response with responsivity of 0.307 A/W at 1,550 nm. Taking both dark current and responsivity into consideration, a high detectivity of 1.37×10^{10} cm·Hz$^{1/2}$/W was achieved which is comparable with commercial Ge photodetector. Meanwhile, its potential for light modulation was experimentally evaluated through characterization of spectral response under varying reverse bias voltages. Significant electric field-dependent photo response was observed from 1,700 to 2,200 nm. The extracted effective absorption coefficient spectral of the GeSn/Ge MQW region show a QCSE behavior. It is the first time that QCSE effect was discovered in GeSn/Ge MQW system. Relatively high absorption ratio ($\Delta\alpha/\alpha_0$) of 1.81 under reverse bias voltage of 2 V was achieved at 2 μm, showing its potential for effective optical modulation.

2. Material characterizations and device fabrication

The GeSn/Ge MQW structure was grown on a 300 mm Si substrate using RPCVD. Before the growth of device layer, a 1 μm strain-relaxed Ge layer was grown as a buffer layer to confine the defects at Ge/Si interface. The n-type and p-type Ge contact layers were realized by in-situ doping during the growth procedure in RPCVD. The intrinsic GeSn/Ge MQW region consists of 15 periods of 20 nm Ge barrier layer and 7.5 nm $Ge_{0.92}Sn_{0.08}$ well layer. The thin GeSn well layer was designed not only to reduce the TDD by preventing strain relaxation, but also to provide better confinement for the excitons. The material quality after growth was characterized by atomic force microscope (AFM) and cross-sectional transmission electron microscopy (TEM) in Fig. 1. The root-mean-square (RMS) roughness obtained from a scanning area of 50×50 μm^2 is 1.04 nm and the achieved roughness is uniform across the entire 300 mm wafer surface. From the cross sectional TEM image, uniform and abrupt interfaces between GeSn and Ge layers are observed which manifest that the as-grown material is of high quality.

X-ray diffraction (XRD) characterization was used to evaluate the strain in the GeSn/Ge MQW region. Figure 2(a) shows the high-resolution XRD rocking curves of the as-grown sample at (004) orientation. The main peaks (from right to left) correspond to Si substrate and relaxed Ge buffer layer respectively. The satellite peaks on the left of Ge peak are uniform and well-defined, revealing a uniform GeSn/Ge MQW structure with high crystalline quality. The asymmetric (115) reciprocal space mapping (RSM) of the GeSn/Ge MQW structure is shown in Fig. 2(b). The diffraction peaks of the GeSn/Ge MQW region have same reciprocal lattice vector Q_x as the strain-relaxed Ge buffer layer, demonstrating that the GeSn layers in the MQW structure are fully strained.

Optics EXPRESS

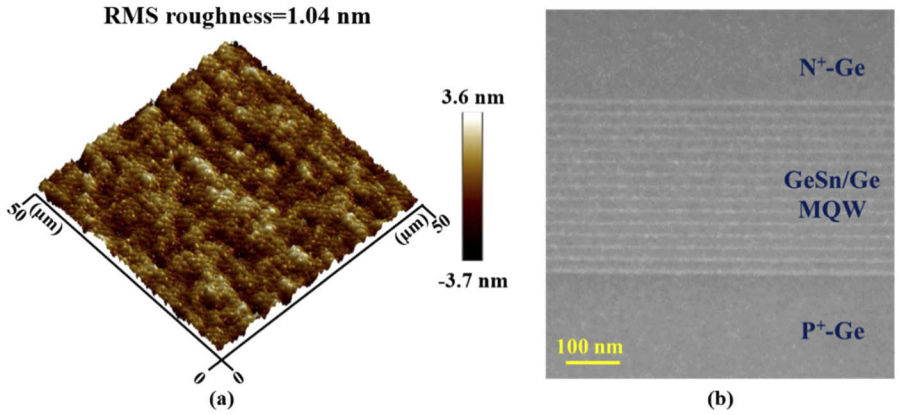

Fig. 1. (a) 3D AFM image of as-grown sample across a scanning area of 50×50 μm^2. (b) Cross-sectional TEM image of the GeSn/Ge MQW *n-i-p* structure.

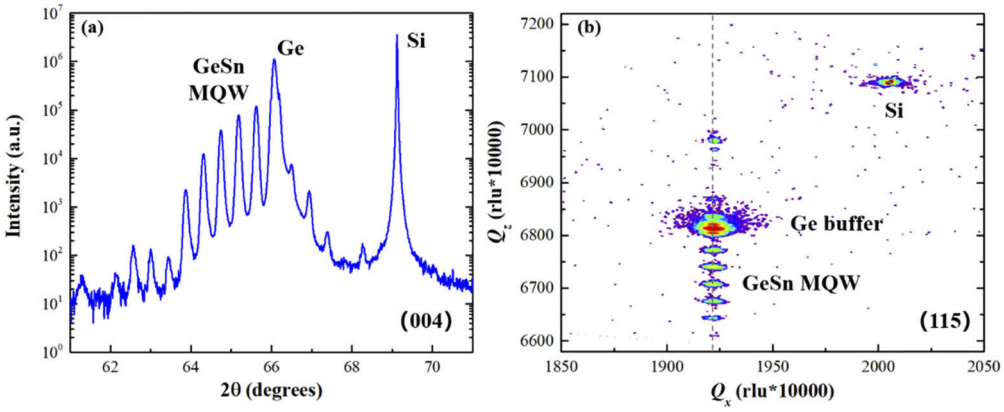

Fig. 2. (a) High resolution XRD rocking curve of GeSn/Ge MQW sample at (004) orientation. (b) Asymmetric (115) reciprocal space mapping of the as-grown wafer.

GeSn/Ge MQW *p-i-n* photodiode with double-mesa structure was fabricated on the as-grown sample. Figure 3(a) shows the three-dimensional (3D) schematic diagram of the designed GeSn/Ge MQW photodiode structure. In the fabrication procedure, top mesas with various diameters were firstly patterned and formed by chlorine-based reactive ion etching (RIE) to expose bottom p^+-Ge region. Bottom mesa was implemented using similar process. This step is for the electrode pads to be formed on the intrinsic Ge buffer layer rather than the heavily-doped p^+-Ge, favorable for high frequency performance. After the formation of double-mesa structure, a ~400 nm SiO_2 was deposited as passivation and isolation layer by plasma enhanced chemical vapor deposition (PECVD) at temperature of 250°C. The contact window was patterned and opened by a combination of fluorine-based dry etching and diluted buffered oxide etch (BOE) wet etching for a decent etching surface. Finally, metal stack of Ti (20 nm)/TiN (50 nm)/Al (300 nm) was patterned and formed by sputtering and lift-off process. The entire process was performed under the temperature of 250°C to avoid Ge-Sn inter-diffusion in the MQW region, which may affect the electrical and optical properties of the devices. The top-view scanning electron microscope (SEM) image of the fabricated device with mesa diameter of 250 μm is shown in Fig. 3(b). The clean surface with well-defined double-mesa structure and standard ground-signal-ground (GSG) electrode pads can be observed clearly.

Optics EXPRESS

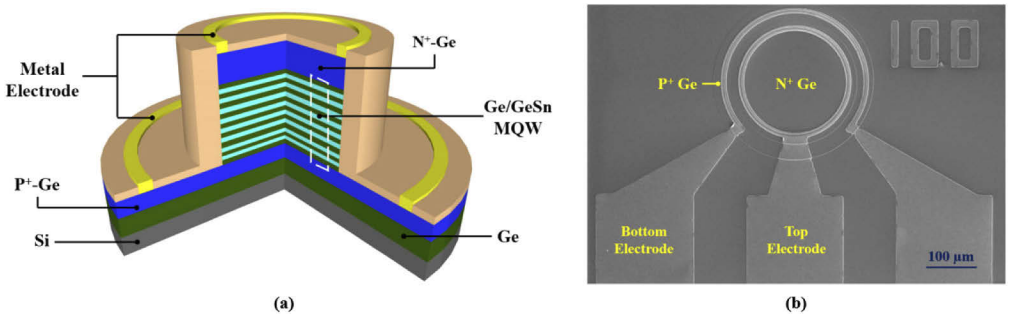

Fig. 3. (a) 3D schematic diagram of GeSn/Ge MQW *p-i-n* photodiode with double-mesa structure. (b) Top-view SEM image of fabricated GeSn/Ge MQW photodiode.

3. Characterizations of photodiode as photodetector

Dark current is one of the pivotal metrics of photodiodes. As shown in Fig. 4(a), dark current was measured from -1 to 1 V on photodiodes with varying mesa diameters. For the photodiode with mesa diameter of 60 μm, high on/off ratio around 5×10^4 was achieved, manifesting excellent rectifying behavior. Low dark current density around 16.3 mA/cm^2 was achieved on a photodiode with mesa diameter of 250 μm. As benchmarked in Fig. 5 [1,3,25–39], such value is among the lowest in GeSn photodiodes. The dark current density usually increases with Sn fraction since higher Sn composition means higher lattice mismatch. To the best of our knowledge, the achieved dark current density is the lowest for GeSn photodiode with Sn composition larger than 4%. The low dark current density is attributed to the low TDD in GeSn/Ge MQW because the GeSn layer is pseudomorphic without strain relaxation. In order to investigate the attribution of dark current density, surface leakage and bulk leakage current densities were extracted according

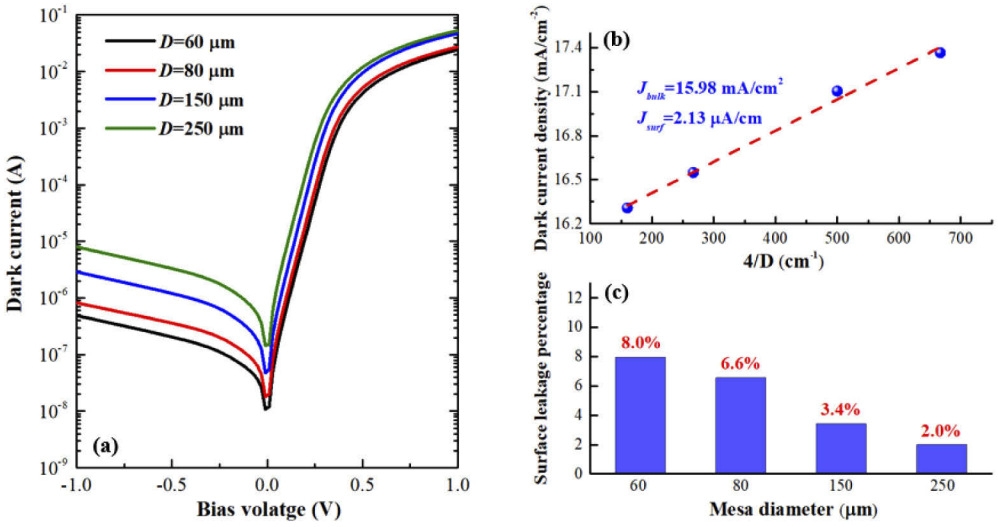

Fig. 4. (a) Dark current characteristics of the GeSn/Ge MQW photodiodes with varying mesa diameters. (b) Linear fitting of dark current density versus 4/D for GeSn/Ge MQW photodiodes allows for extraction of bulk and surface leakage densities. (c) Surface leakage percentages of fabricated photodiodes with varying mesa diameters.

Optics EXPRESS

to the following equation:

$$J_{dark} = J_{bulk} + \frac{4}{D} J_{surf} \tag{1}$$

where D is the mesa diameter and $4/D$ is known as perimeter-to-area ratio. The extracted bulk leakage and surface leakage current densities from linear interpolation in Fig. 4(b) are 15.98 mA/cm^2 and 2.13 μA/cm, respectively. The surface leakage mainly originates from minority carriers and current flows on the sidewall, while the bulk leakage is related to material defects. The percentages of surface leakage were plotted in Fig. 4(c). The photodiode with smaller mesa diameter has higher surface leakage percentage due to increased perimeter-to-area ratio. Owing to effective passivation methods, surface leakage percentages for all photodiodes are smaller than 10%. Even though the MQW structure is beneficial for low TDD, bulk leakage still dominates dark current. The bulk leakage probably derives from the migration of threading dislocation at Ge/Si interface. For group IV material, lattice mismatch is always an intractable issue and the degraded performance as compared with III-V material is mainly rooted on it.

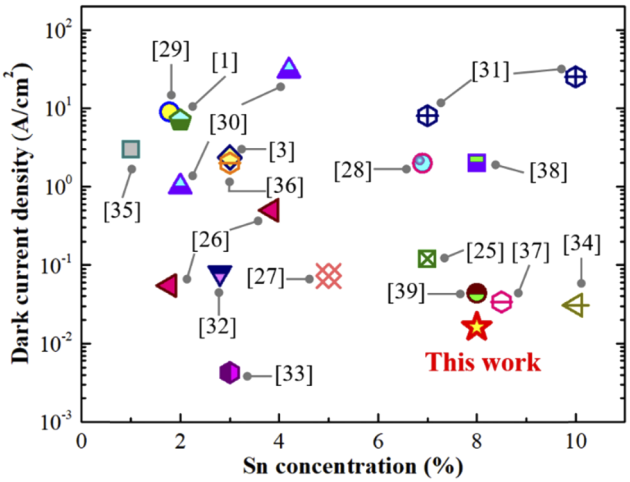

Fig. 5. Benchmarking of the dark current density for GeSn photodiodes grown on Si substrate at bias voltage of -1 V.

The dark current characteristic of the photodiode can be expressed using the Shockley equation:

$$I = I_0 \exp\left[\frac{q(V - R_s I_{net})}{nkT}\right] + \frac{V}{R_{sh}} \tag{2}$$

where I_0 is reverse saturation current, n is ideality factor, R_s and R_{sh} are series resistance and shunt resistance respectively. Near 0 V, the equation can be simplified as $I = I_0 + V/R_{sh}$ and R_{sh} can be extracted by dV/dI. The shunt resistances at room temperature (T=300 K) for photodiode with mesa diameters of 60 and 250 μm are 111 and 82.2 kΩ, respectively. The high shunt resistances achieved are consistent with low surface leakage density and further indicate the effective surface passivation. After obtaining shunt resistance, the ideality factor n and series resistance R_s can be extracted using the transformed expression: $dV/dI_{net} = (nkT/q)I_{net}^{-1} + R_s$ where the net current flow I_{net} can be calculated using $I_{net} = I - V/R_{sh}$. As shown in Fig. 6, the extracted ideality factors for both photodiodes are around 1.29 which is close to an ideal *pn* junction. The extracted series resistances are 26.4 and 13.4 Ω for photodiode with mesa diameters of 60 and 250 μm, respectively. The low series resistance is beneficial for high speed operation due to the reduced resistance-capacitance (RC) delay.

Optics EXPRESS

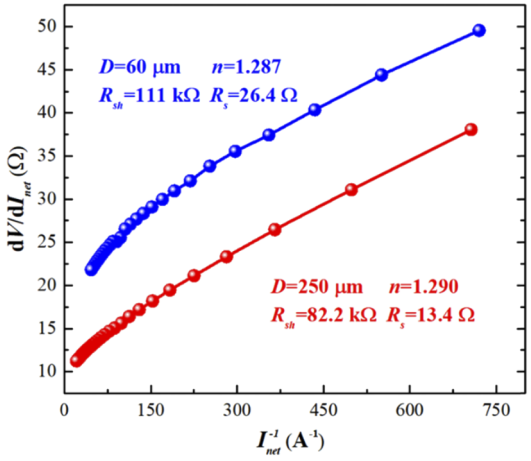

Fig. 6. Linear fitting of I_{net}^{-1} versus dV/dI_{net} allows for the extraction of series resistance R_S and ideality factor n for GeSn/Ge MQW photodiodes with mesa diameter of 60 and 250 μm.

Photo current was characterized at two essential communication bands: 1,550 and 2,000 nm, respectively. Before the measurement, the propagation loss in the fibers and the coupling loss in the connectors were calibrated. As shown in Fig. 7(a), the calibrated optical power varies from 0.73 to 5.14 mW at 1,550 nm. The flat response curves under reverse bias suggest the effective collection of photon-generated carriers. The relationship between optical power and photo current at -1 V was plotted in Fig. 8(a). Relatively high responsivity around 0.307 A/W was achieved by linear interpolation. Similarly, the optical response of the photodiode at 2 μm was measured and extrapolated in Fig. 7(b) and Fig. 8(b). The slight deviation in the linear interpolation probably attributes to the increased loss between input fiber and photodiode surface.

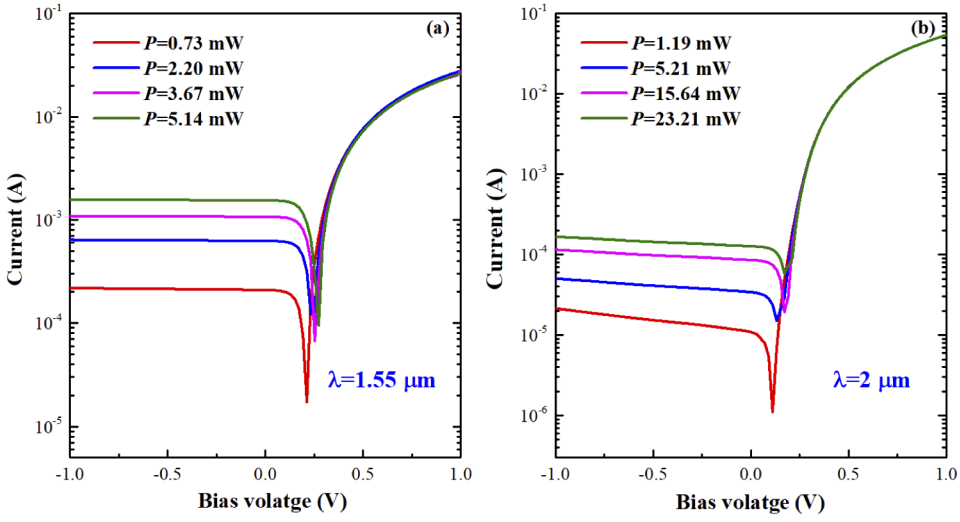

Fig. 7. Current-voltage (*I-V*) characteristics of the GeSn/Ge MQW photodiode at incident wavelength of (a) 1,550 nm with varying optical power from 0.73 to 5.14 mW and (b) 2 μm with varying optical power from 1.19 to 23.21 mW.

Optics EXPRESS

At 2 μm, the extracted responsivity is 0.007 A/W. The optical performance manifests that the GeSn/Ge MQW photodiode is capable of photo detection from 1,550 to 2,000 nm.

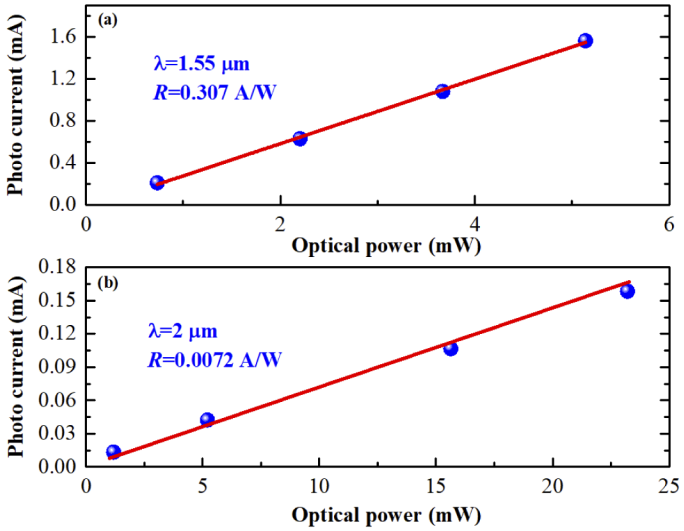

Fig. 8. Linear fitting of photocurrent versus optical power at (a) 1,550 nm and (b) 2 μm.

The relatively low responsivity at 2 μm is reasonable because the total thickness of absorptive GeSn layers in the MQW region is only 112.5 nm. Moreover, the bandgap of GeSn layer in MQW structure increases due to the compressive strain and quantum confined effect. The band structure of the GeSn/Ge MQW was calculated using single band approximation. In the calculation, the Ge layer was treated as fully relaxed and the in-plain and normal strain in GeSn layer is around -0.0116 and 0.0088. The energy shifts introduced by strain were modeled by deformation potential theory. Taking the energy shift caused by strain into consideration, the band offsets for Γ valley, L valley, heavy hole and light hole bands were calculated, respectively. The eigenvalues and wave functions were obtained by solving one dimensional time independent Schrödinger's equation:

$$-\frac{h^2}{8\pi^2 m^*}\frac{\partial^2 \phi_n}{\partial z^2} + V(z)\phi_n = E_n\phi_n \tag{3}$$

where the index n represents the n^{th} band state in the quantum well, $V(z)$ is the band offset obtained in the previous calculation and m^* is the effective carrier mass for different energy bands. The calculation results were plotted in Fig. 9. The direct bandgap ($E_{\Gamma 1}$-E_{hh1}) in the GeSn well region is around 0.66 eV which corresponds to a wavelength of 1,880 nm. It explains the relatively low responsivity at 2 μm since weak indirect bandgap absorption is dominant at this wavelength.

The specific detectivity D^* was calculated to compare the performance of GeSn/Ge MQW photodiode with commercial Ge and extended-InGaAs photodetectors operating at similar wavelength range in Fig. 10. Due to the low dark current in pseudomorphic GeSn/Ge MQW region, the shot noise current achieved in this work is around 2.15×10^{-13} A·Hz$^{-1/2}$ when the input optical power is close to 0. It should be noted that all the measurements performed in this work were at room temperature (T=300 K). The calculated specific detectivity D^* at 1,550 nm is 1.37×10^{10} cm·Hz$^{1/2}$/W which is two orders higher than bulk $Ge_{0.9}Sn_{0.1}$ photodetector in Ref. [31]. The achieved specific detectivity at C-band makes the GeSn/Ge MQW photodiode in this work competitive as compared with commercial Ge and extended-InGaAs photodetectors. At 2 μm, the specific detectivity is 3.20×10^{8} cm·Hz$^{1/2}$/W due to the relatively low responsivity as

Optics EXPRESS

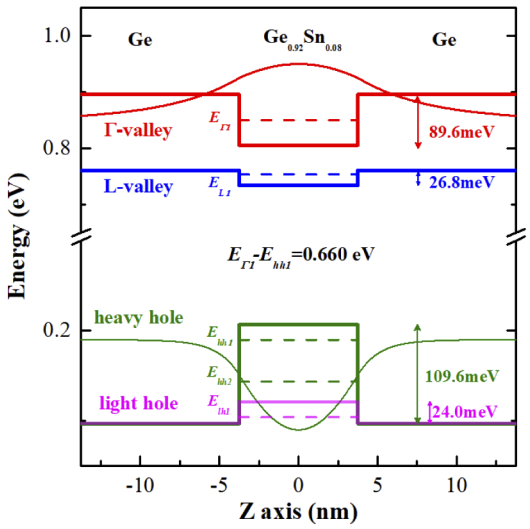

Fig. 9. Band structure between Ge barrier layer and $Ge_{0.92}Sn_{0.08}$ well layer calculated using single band model. Ground states in each bands were represented using dashed lines.

explained before. The relatively low detectivity at 2 μm can be optimized by increasing the Sn concentration to reduce the bandgap of GeSn or increasing the thickness of GeSn well region to weaken the quantum confined effect. It is desirable to realize high detectivity across the entire range from 1,550 to 2,000 nm using the optimized GeSn/Ge MQW structure in the future.

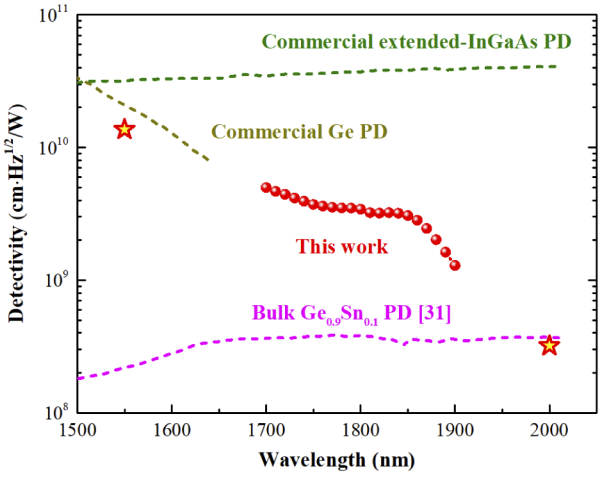

Fig. 10. Comparison of specific detectivity D* of fabricated GeSn/Ge *p-i-n* photodiode with commercial extended-InGaAs photodetector, commercial Ge photodetector and bulk $Ge_{0.9}Sn_{0.1}$ photodetector [31] from 1,500 to 2,000 nm.

4. Characterizations of photodiode as modulator

To investigate the modulation effect in the GeSn/Ge MQW photodiode, the spectral response was obtained from 1,700 to 2,200 nm at varying reverse bias voltages in Fig. 11. Since the calculated direct bandgap of the GeSn well region is 0.66 eV (1,880 nm), the measured wavelength range has

Optics EXPRESS

covered the direct bandgap. It can be observed that the spectral response is bias voltage-dependent. At a reverse bias voltage of 2 V, the achieved responsivities are the highest across the entire measurement range. In terms of reverse bias voltages of 0.5, 1, 1.5 V, there is a cross-over region between 1,820 to 1,860 nm where the responsivity does not increase with bias voltage. In order to understand the physical mechanism behind the spectral response, absorption coefficient of GeSn layer in the MQW region was extracted according to the following equation:

$$R_{opt} = (1 - R)\frac{e\lambda}{hc}e^{-\alpha_{n-Ge}t_{n-Ge}}(1 - e^{-\alpha_{Ge}t_{Ge}}e^{-\alpha_{GeSn}t_{GeSn}}) \quad (4)$$

where R_{opt} is responsivity, R is reflection, and α_{Ge} and α_{GeSn} are the absorption coefficient of Ge and GeSn respectively. The absorption coefficient for n^+ doped Ge region is assumed as same as intrinsic Ge region and α_{Ge} was obtained using ellipsometer on a bulk Ge wafer. The assumption is reasonable since the absorption coefficient of Ge is very small (< 100/cm) at this wavelength range. The reflection spectrum was measured using microscope Fourier-transform infrared spectroscopy (FTIR) in Fig. 12. Standard gold film was used to calibrate the reflection in the measurement. It can be observed that resonance behavior exists in the reflection spectrum. The resonance peaks are attributed to air-Ge-Si cavity structure since the refractive index of $Ge_{0.92}Sn_{0.08}$ is close to Ge. According to the position of resonance peaks, the total thickness of Ge layer (device layer + Ge buffered layer) is estimated to be 2.48 μm which is close to the proposed thickness in the material growth.

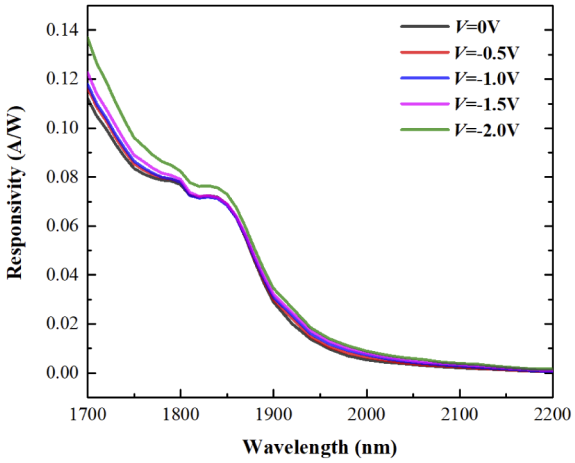

Fig. 11. Spectral response of GeSn/Ge MQW photodiode from 1,700 to 2,200 nm at reverse bias voltage of 0, 0.5, 1, 1.5 and 2 V respectively.

The absorption coefficient spectral of GeSn layer in the MQW region were extracted from 0.57 to 0.73 eV at varying voltages in Fig. 13(a). It can be observed that the absorption spectral can be divided into three regions: indirect bandgap absorption, Urbach tail and direct bandgap absorption. Direct bandgap and indirect bandgap absorption are two typical inter-band transition in semiconductors. Urbach tail is related to the transition between band tail states such as doping and defects energy states which are exactly above the valence band or below the conduction band [40]. The absorption from Urbach tail could be dominant when the $E_g^{indirect} < h\nu < E_g^{direct}$ since the indirect bandgap absorption is very weak. However, it is noted that the direct bandgap absorption region is not as smooth as expected. Small peak was observed in the direct bandgap absorption regions at all reverse bias voltages. In terms of direct bandgap transition, it satisfies

Optics EXPRESS

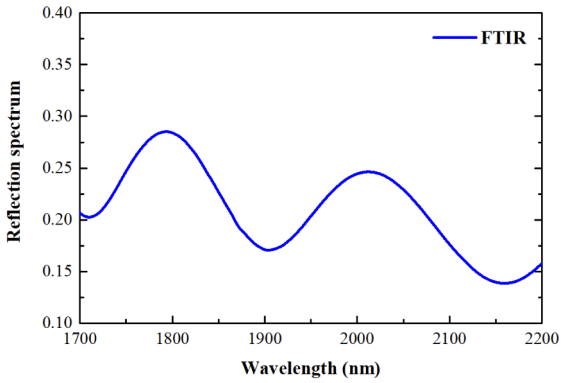

Fig. 12. Micro-FTIR reflection spectrum of fabricated GeSn/Ge MQW photodiode from 1,700 to 2,200 nm.

the following equation near the band edge:

$$(\alpha h\nu)^2 = A(h\nu - E_g) \tag{5}$$

where A is a constant and $h\nu$ is the energy of incident photons. Using this equation, the direct bandgap of GeSn layer was extrapolated at 0 V in Fig. 13(b). The extracted direct bandgap in the quantum well is around 0.693 eV which is close to the calculated value of 0.660 eV before.

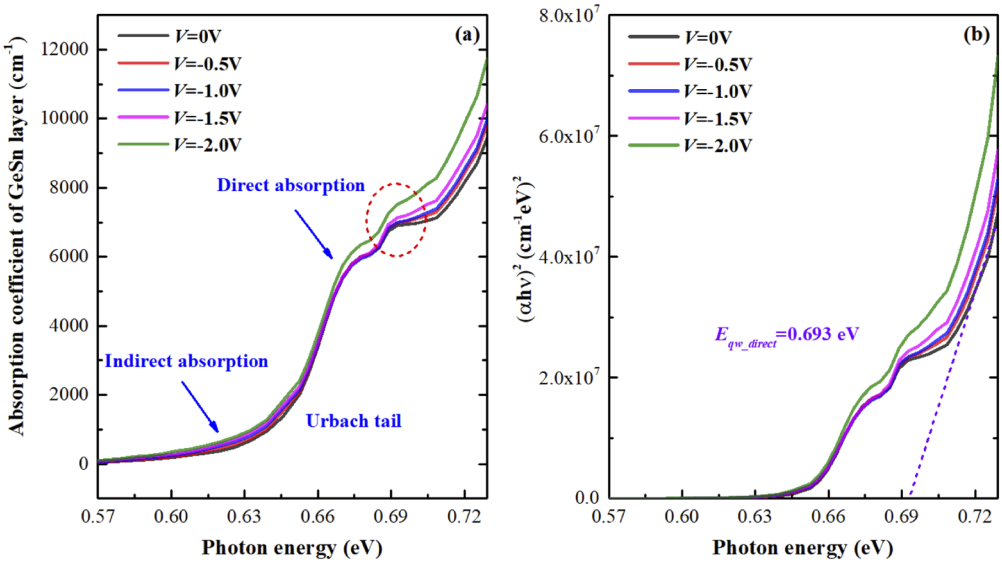

Fig. 13. (a) Extracted absorption coefficient spectral of GeSn layer in the MQW region at varying reverse bias voltage. (b) Linear fitting of $(\alpha h\nu)^2$ versus photon energy $h\nu$ allows for extraction of direct bandgap of GeSn well layer at 0 V.

In order to investigate the mechanism behind the small peak in the direct bandgap absorption region, GeSn/Ge MQW layer was treated as a whole and the photon absorption was separated into two parts: absorption within and outside the depletion region. Therefore, the effective absorption coefficient of GeSn/Ge MQW layer can be extrapolated using the following equation:

$$R_{opt} = (1-R)\frac{e\lambda}{hc}e^{-\alpha_{n-Ge}t_{n-Ge}}(1-e^{-\alpha_v t_d}e^{-\alpha_0(t_i-t_d)}) \tag{6}$$

Optics EXPRESS

where t_d is the thickness of depletion region, t_i is the total thickness of the intrinsic MQW region and α_0 and α_v are effective absorption coefficients of GeSn/Ge MQW at 0 V and any other reverse bias V. The thickness of depletion region can be obtained through C-V measurement by $d=\varepsilon_i A/C_j$ because the photodiode can be regarded as a parallel capacitor. The total capacitance C obtained from C-V measurement is composed of parasitic capacitance C_p and junction capacitance C_j. Since the junction capacitance is proportional to the mesa area, the parasitic capacitance C_p=4.69 pF can be extracted from the linear interpolation in Fig. 14.

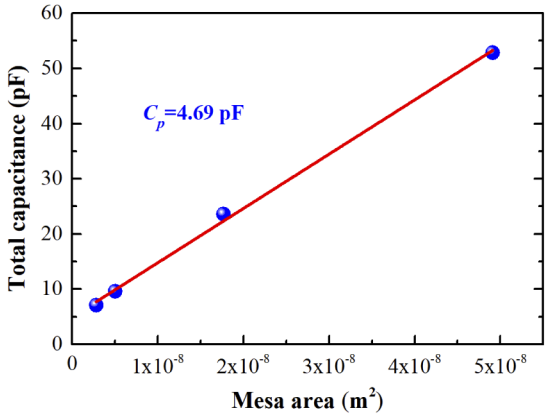

Fig. 14. Linear fitting of total capacitance versus mesa area allows for extraction of parasitic capacitance C_p.

After obtaining junction capacitance and thickness of depletion region, the effective absorption coefficient of GeSn/Ge MQW was calculated and plotted in Fig. 15. It is noteworthy that small peaks close to the direct bandgap of GeSn well layer can be observed in the absorption spectral. The small peaks probably originate from the exciton absorption in the MQW structure due to QCSE effect. The binding energy of exciton in the quantum well can be described using the equation:

$$E_{exciton}^{n} = \frac{e^4}{8\varepsilon^2 h^2}\left(\frac{m_e m_h}{m_e + m_h}\right)\frac{1}{(n-1/2)^2} \tag{7}$$

where m_e and m_h are effective masses of electron and hole respectively. For the excitons confined at Γ valley and heavy hole band, the parameters used here are consistent with band structure calculation: m_e=0.0316 m_0 and m_h=0.223 m_0. The calculated binding energy is around 5.63 meV which roughly satisfies the energy difference $E_{exciton} = E_{qw\_direct}$ - $E_{binding}$. Moreover, the peak position shifts to lower photon energy with increasing reverse bias voltage which is also one of the characteristics of QCSE effect. In the GeSn/Ge MQW structure, the well region is 7.5 nm which provides relatively sufficient confinement for the exciton. However, the exciton absorption is weak in this work due to the following two possible reasons. One of the reasons is that the material defects in the GeSn/Ge MQW region is not as low as expected. Even though the GeSn layer is pseudomorphic, the defects at Ge/Si interface can still propagate into the device region which is also the cause of large percentage of bulk leakage as discussed before. Such problem can be solved by direct wafer bonding (DWB) process after the material growth [41]. The defective Ge buffer layer can be etched away by transferring the sample on an insulator platform. The other reason could be related to the measurement limitation. The resolution of optical filter is 10 nm and the applied reverse bias voltage is relatively low. Since the total thickness of the MQW region is 412.5 nm, the electric field density in the MQW region is not sufficiently strong to bring significant shift of the exciton peak. In addition, all the measurements were performed at room temperature. The thermal perturbation at room temperature (kT = 25.8 meV) is destructive for

Optics EXPRESS

the excitons due to the low binding energy. Even though the exciton peak in this work is not remarkable, it is the first time that QCSE effect was discovered in GeSn/Ge system. With further optimization in the material growth or switching the barrier material to SiGeSn, more prominent QCSE effect and high efficiency modulation based on exciton absorption can be realized.

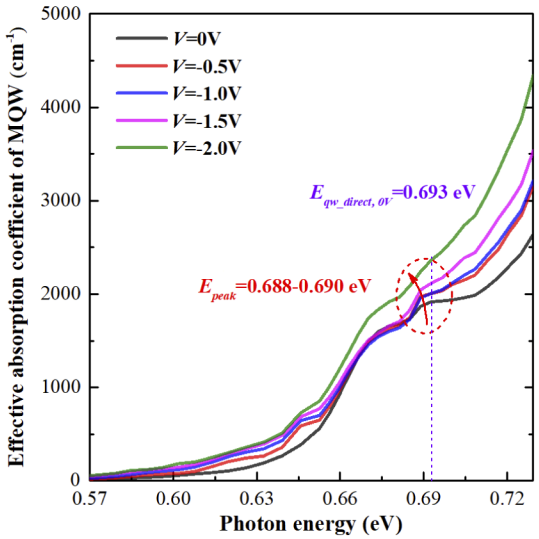

Fig. 15. Extracted effective absorption coefficient of GeSn/Ge MQW region at varying reverse bias voltage from 0.57 to 0.73 eV.

To achieve effective optical modulation, the deviation of absorption coefficient for a given reverse bias voltage is pivotal. The change of absorption coefficient can be evaluated by absorption ratio which is defined as $\Delta\alpha/\alpha_0$. Here, the effective absorption coefficient of the GeSn/Ge MQW was used in the calculation. As shown in Fig. 16, the absorption ratios at all bias voltages decrease first and then increase. When the reverse bias voltage is lower than 2 V, the absorption ratio turns

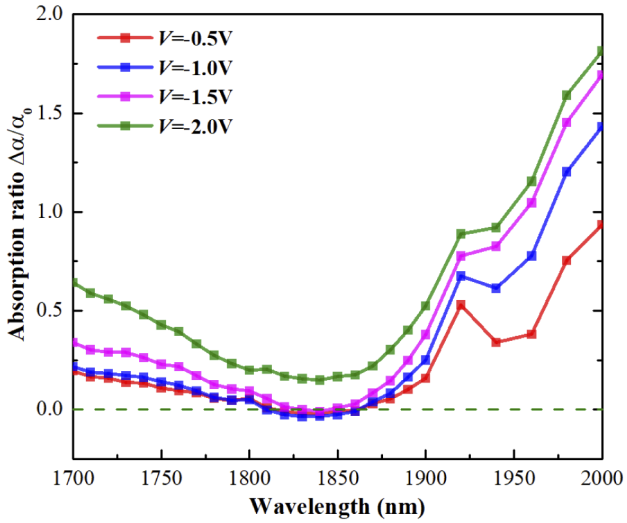

Fig. 16. Change of absorption ratio of GeSn/Ge MQW region at varying reverse bias from 1,700 to 2,000 nm.

Optics EXPRESS

into negative around 1,830 nm and then returns to positive value at longer wavelength. At voltage of -2 V, the absorption ratio remains positive across the entire range from 1,700 to 2,000 nm and the maximum value is around 1.81 at 2 μm, showing promise for optical modulation at 2 μm band.

The 3-dB bandwidth of GeSn/Ge MQW photodiode was calculated theoretically in Fig. 17. In the calculation, both transit-limited bandwidth and RC delay-limited bandwidth were taken into consideration. By assuming the velocity of electron in depletion region has reached the saturation velocity v_{sat}=6×10^6 cm/s, the transit-limited bandwidth can be calculated using $f_T = 0.45v_{sat}/d_i$ [42]. The RC delay limited bandwidth is dominant for device with large surface area and it can be expressed by f_{RC}=1/(2π(R_s+R_l)(C_j+C_p)). The load resistance R_l was estimated to be 50 Ω and the values of series resistance R_s, junction capacitance C_j and parasitic capacitance C_p had been obtained in the former discussion. As shown in Fig. 17, the theoretical 3-dB bandwidth for the photodiode with mesa diameter of 30 μm can reach 12 GHz at -2 V. The theoretical calculation could overestimate the 3-dB bandwidth of the photodiode since the carrier trapping effect in the MQW was not taken into consideration. However, the carrier trapping effect will be alleviated at higher bias voltage because of narrower barrier. Therefore, the GeSn/Ge photodiode fabricated in this work is believed to be capable of high frequency operation.

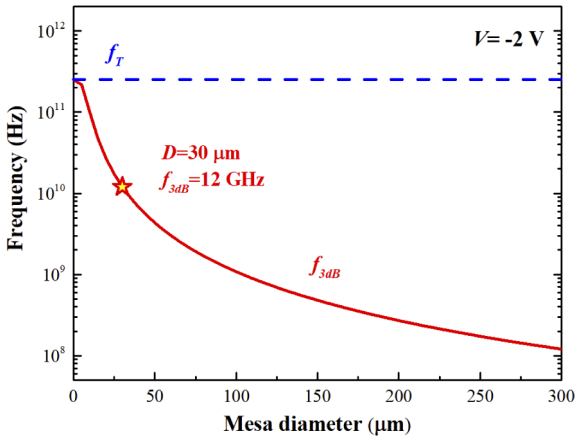

Fig. 17. Theoretically calculated 3-dB bandwidth of fabricated GeSn/Ge MQW photodiode as a function of mesa diameter. The blue dashed line represents transit-limited bandwidth.

5. Conclusion

The photo detection and modulation performance of GeSn/Ge MQW *p-i-n* photodiode was investigated. The GeSn/Ge MQW *p-i-n* structure was grown on a 300-mm Ge-buffered Si substrate by RPCVD which is promising for large-scale production. High material quality with uniform and pseudomorphic GeSn well layers was verified by TEM and XRD characterization. As a photodetector, the fabricated GeSn/Ge MQW photodiode shows an ultralow dark current of 16.3 mA/cm^2 at -1 V and a high responsivity of 0.307 A/W at 1,550 nm. The achieved specific detectivity at C-band (centered at 1,550 nm) is 1.37×10^{10} cm·Hz$^{1/2}$/W which is comparable with commercial Ge and extended-InGaAs photodetectors. The potential of GeSn/Ge MQW photodiode as optical modulator was also investigated from 1,700 to 2,200 nm. QCSE effect was observed in the effective absorption coefficient spectra of the GeSn/Ge MQW region. The exciton peak shifts from 0.690 to 0.688 eV when the reverse bias voltage increases from 0 to 2 V. The achieved absorption ratio under -2 V at 2 μm is 1.81, manifesting the fabricated GeSn/Ge MQW can be used as a modulator operating at 2 μm. This work paves a way for the application

Optics EXPRESS

of GeSn/Ge MQW photodiodes as photo detectors and optical modulators in the optoelectronic integrated circuits.

Funding

National Research Foundation Singapore (NRF–CRP19–2017–01); Ministry of Education - Singapore (R-263-000-D45-112); Ministry of Education - Singapore (R-263-000-C58-133).

Acknowledgments

The authors acknowledge Dr. Chong Gang Yih and Ms. Ngo Ling Ling in Nanyang Technological University for the help in sputtering and PECVD.

Disclosures

The authors declare that there are no conflicts of interest related to this article.

References

1. J. Mathews, R. Roucka, J. Xie, S.-Q. Yu, J. Menéndez, and J. Kouvetakis, "Extended performance GeSn/Si (100) p-i-n photodetectors for full spectral range telecommunication applications," Appl. Phys. Lett. **95**(13), 133506 (2009).
2. J. Werner, M. Oehme, M. Schmid, M. Kaschel, A. Schirmer, E. Kasper, and J. Schulze, "Germanium-tin pin photodetectors integrated on silicon grown by molecular beam epitaxy," Appl. Phys. Lett. **98**(6), 061108 (2011).
3. S. Su, B. Cheng, C. Xue, W. Wang, Q. Cao, H. Xue, W. Hu, G. Zhang, Y. Zuo, and Q. Wang, "GeSn pin photodetector for all telecommunication bands detection," Opt. Express **19**(7), 6400–6405 (2011).
4. H. Tran, T. Pham, J. Margetis, Y. Zhou, W. Dou, P. C. Grant, J. M. Grant, S. Alkabi, W. Du, and G. Sun, "Study of High Performance GeSn Photodetectors with Cutoff Wavelength Up to 3.7 μm for Low-Cost Infrared Imaging," in *2019 Conference on Lasers and Electro-Optics (CLEO)*, (IEEE, 2019), 1–2.
5. H. Zhang, N. Kavanagh, Z. Li, J. Zhao, N. Ye, Y. Chen, N. Wheeler, J. Wooler, J. Hayes, and S. Sandoghchi, "100 Gbit/s WDM transmission at 2 μm: transmission studies in both low-loss hollow core photonic bandgap fiber and solid core fiber," Opt. Express **23**(4), 4946–4951 (2015).
6. P. Roberts, F. Couny, H. Sabert, B. Mangan, D. Williams, L. Farr, M. Mason, A. Tomlinson, T. Birks, and J. Knight, "Ultimate low loss of hollow-core photonic crystal fibres," Opt. Express **13**(1), 236–244 (2005).
7. Z. Li, A. Heidt, J. Daniel, Y. Jung, S. Alam, and D. J. Richardson, "Thulium-doped fiber amplifier for optical communications at 2 μm," Opt. Express **21**(8), 9289–9297 (2013).
8. Z. Li, A. Heidt, N. Simakov, Y. Jung, J. Daniel, S. Alam, and D. Richardson, "Diode-pumped wideband thulium-doped fiber amplifiers for optical communications in the 1800–2050nm window," Opt. Express **21**(22), 26450–26455 (2013).
9. H. Zhang, Z. Li, N. Kavanagh, J. Zhao, N. Ye, Y. Chen, N. Wheeler, J. Wooler, J. Hayes, and S. Sandoghchi, "81 Gb/s WDM transmission at 2μm over 1.15 km of low-loss hollow core photonic bandgap fiber," in *2014 The European Conference on Optical Communication (ECOC)*, (IEEE, 2014), 1–3.
10. D. J. Richardson, "Filling the light pipe," Science **330**(6002), 327–328 (2010).
11. S. Xu, K. Han, Y.-C. Huang, K. H. Lee, Y. Kang, S. Masudy-Panah, Y. Wu, D. Lei, Y. Zhao, and H. Wang, "Integrating GeSn photodiode on a 200 mm Ge-on-insulator photonics platform with Ge CMOS devices for advanced OEIC operating at 2 μm band," Opt. Express **27**(19), 26924–26939 (2019).
12. H. Zhou, S. Xu, Y. Lin, Y.-C. Huang, B. Son, W. Li, X. Guo, L. Liu, K. H. Lee, and X. Gong, "High-efficiency photo detection at 2 μm realized by GeSn/Ge multiple-quantum-well photodetectors with photon-trapping microstructure," in *CLEO: Science and Innovations*, (Optical Society of America, 2020), STh4L. 1.
13. H. Tran, T. Pham, W. Du, Y. Zhang, P. C. Grant, J. M. Grant, G. Sun, R. A. Soref, J. Margetis, and J. Tolle, "High performance Ge0. 89Sn0. 11 photodiodes for low-cost shortwave infrared imaging," J. Appl. Phys. **124**(1), 013101 (2018).
14. H. Tran, T. Pham, J. Margetis, Y. Zhou, W. Dou, P. C. Grant, J. M. Grant, S. Al-Kabi, G. Sun, and R. A. Soref, "Si-based GeSn photodetectors toward mid-infrared imaging applications," ACS Photonics **6**(11), 2807–2815 (2019).
15. H. Zhou, S. Xu, Y. Lin, Y.-C. Huang, B. Son, Q. Chen, X. Guo, K. H. Lee, S. C.-K. Goh, and X. Gong, "High-efficiency GeSn/Ge multiple-quantum-well photodetectors with photon-trapping microstructures operating at 2 μm," Opt. Express **28**(7), 10280–10293 (2020).
16. S. Wirths, R. Geiger, N. Von Den Driesch, G. Mussler, T. Stoica, S. Mantl, Z. Ikonic, M. Luysberg, S. Chiussi, and J. Hartmann, "Lasing in direct-bandgap GeSn alloy grown on Si," Nat. Photonics **9**(2), 88–92 (2015).
17. M. Oehme, K. Kostecki, M. Schmid, M. Kaschel, M. Gollhofer, K. Ye, D. Widmann, R. Koerner, S. Bechler, and E. Kasper, "Franz-Keldysh effect in GeSn pin photodetectors," Appl. Phys. Lett. **104**(16), 161115 (2014).
18. S. Bechler, M. Oehme, O. Latzel, M. Schmid, K. Kostecki, R. Koerner, M. Gollhofer, E. Kasper, and J. Schulze, "Franz-Keldysh Effect in GeSn Detectors," ECS Trans. **64**(6), 383–390 (2014).

Optics EXPRESS

19. A. Elbaz, D. Buca, N. von den Driesch, K. Pantzas, G. Patriarche, N. Zerounian, E. Herth, X. Checoury, S. Sauvage, and I. Sagnes, "Ultra-low-threshold continuous-wave and pulsed lasing in tensile-strained GeSn alloys," Nat. Photonics **14**(6), 375–382 (2020).
20. D. Stange, N. Von Den Driesch, D. Rainko, C. Schulte-Braucks, S. Wirths, G. Mussler, A. Tiedemann, T. Stoica, J. Hartmann, and Z. Ikonic, "Study of GeSn based heterostructures: towards optimized group IV MQW LEDs," Opt. Express **24**(2), 1358–1367 (2016).
21. Y. Zhou, Y. Miao, S. Ojo, H. Tran, G. Abernathy, J. M. Grant, S. Amoah, G. Salamo, W. Du, and J. Liu, "Electrically injected GeSn lasers on Si operating up to 100 K," arXiv preprint arXiv:2004.09402 (2020).
22. B. Son, Y. Lin, K. H. Lee, Q. Chen, and C. S. Tan, "Dark current analysis of germanium-on-insulator vertical pin photodetectors with varying threading dislocation density," J. Appl. Phys. **127**(20), 203105 (2020).
23. Y.-H. Kuo, Y. K. Lee, Y. Ge, S. Ren, J. E. Roth, T. I. Kamins, D. A. Miller, and J. S. Harris, "Strong quantum-confined Stark effect in germanium quantum-well structures on silicon," Nature **437**(7063), 1334–1336 (2005).
24. Y.-H. Kuo, Y. K. Lee, Y. Ge, S. Ren, J. E. Roth, T. I. Kamins, D. A. Miller, and J. S. Harris, "Quantum-confined Stark effect in Ge/SiGe quantum wells on Si for optical modulators," IEEE J. Sel. Top. Quantum Electron. **12**(6), 1503–1513 (2006).
25. S. Xu, Y.-C. Huang, K. H. Lee, W. Wang, Y. Dong, D. Lei, S. Masudy-Panah, C. S. Tan, X. Gong, and Y.-C. Yeo, "GeSn lateral pin photodetector on insulating substrate," Opt. Express **26**(13), 17312–17321 (2018).
26. H. Tseng, H. Li, V. Mashanov, Y. Yang, H. Cheng, G. Chang, R. Soref, and G. Sun, "GeSn-based pin photodiodes with strained active layer on a Si wafer," Appl. Phys. Lett. **103**(23), 231907 (2013).
27. M. Oehme, K. Kostecki, K. Ye, S. Bechler, K. Ulbricht, M. Schmid, M. Kaschel, M. Gollhofer, R. Körner, and W. Zhang, "GeSn-on-Si normal incidence photodetectors with bandwidths more than 40 GHz," Opt. Express **22**(1), 839–846 (2014).
28. M. Oehme, D. Widmann, K. Kostecki, P. Zaumseil, B. Schwartz, M. Gollhofer, R. Koerner, S. Bechler, M. Kittler, and E. Kasper, "GeSn/Ge multiquantum well photodetectors on Si substrates," Opt. Lett. **39**(16), 4711–4714 (2014).
29. Y.-H. Peng, H. Cheng, V. I. Mashanov, and G.-E. Chang, "GeSn pin waveguide photodetectors on silicon substrates," Appl. Phys. Lett. **105**(23), 231109 (2014).
30. Y. Dong, W. Wang, D. Lei, X. Gong, Q. Zhou, S. Y. Lee, W. K. Loke, S.-F. Yoon, E. S. Tok, and G. Liang, "Suppression of dark current in germanium-tin on silicon pin photodiode by a silicon surface passivation technique," Opt. Express **23**(14), 18611–18619 (2015).
31. T. Pham, W. Du, H. Tran, J. Margetis, J. Tolle, G. Sun, R. A. Soref, H. A. Naseem, B. Li, and S.-Q. Yu, "Systematic study of Si-based GeSn photodiodes with 2.6 µm detector cutoff for short-wave infrared detection," Opt. Express **24**(5), 4519–4531 (2016).
32. Y.-H. Huang, G.-E. Chang, H. Li, and H. Cheng, "Sn-based waveguide pin photodetector with strained GeSn/Ge multiple-quantum-well active layer," Opt. Lett. **42**(9), 1652–1655 (2017).
33. M. Morea, C. E. Brendel, K. Zang, J. Suh, C. S. Fenrich, Y.-C. Huang, H. Chung, Y. Huo, T. I. Kamins, and K. C. Saraswat, "Passivation of multiple-quantum-well Ge0. 97Sn0. 03/Ge pin photodetectors," Appl. Phys. Lett. **110**(9), 091109 (2017).
34. Y. Dong, W. Wang, S. Xu, D. Lei, X. Gong, X. Guo, H. Wang, S.-Y. Lee, W.-K. Loke, and S.-F. Yoon, "Two-micron-wavelength germanium-tin photodiodes with low dark current and gigahertz bandwidth," Opt. Express **25**(14), 15818–15827 (2017).
35. J. Mathews, R. Roucka, C. Weng, R. Beeler, J. Tolle, J. Menéndéz, and J. Kouvetakis, "Near IR photodiodes with tunable absorption edge based on Ge1-y Sny alloys integrated on silicon," ECS Trans. **33**(6), 765–773 (2019).
36. M. Oehme, M. Schmid, M. Kaschel, M. Gollhofer, D. Widmann, E. Kasper, and J. Schulze, "GeSn pin detectors integrated on Si with up to 4% Sn," Appl. Phys. Lett. **101**(14), 141110 (2012).
37. W. Wang, S. Vajandar, S. L. Lim, Y. Dong, V. R. D'Costa, T. Osipowicz, E. S. Tok, and Y.-C. Yeo, "In-situ gallium-doping for forming p+ germanium-tin and application in germanium-tin pin photodetector," J. Appl. Phys. **119**(15), 155704 (2016).
38. H. Cong, C. Xue, J. Zheng, F. Yang, K. Yu, Z. Liu, X. Zhang, B. Cheng, and Q. Wang, "Silicon based GeSn pin photodetector for SWIR detection," IEEE Photonics J. **8**(5), 1–6 (2016).
39. S. Xu, W. Wang, Y.-C. Huang, Y. Dong, S. Masudy-Panah, H. Wang, X. Gong, and Y.-C. Yeo, "High-speed photo detection at two-micron-wavelength: technology enablement by GeSn/Ge multiple-quantum-well photodiode on 300 mm Si substrate," Opt. Express **27**(4), 5798–5813 (2019).
40. H. Tran, W. Du, S. A. Ghetmiri, A. Mosleh, G. Sun, R. A. Soref, J. Margetis, J. Tolle, B. Li, and H. A. Naseem, "Systematic study of Ge1− xSnx absorption coefficient and refractive index for the device applications of Si-based optoelectronics," J. Appl. Phys. **119**(10), 103106 (2016).
41. K. H. Lee, S. Bao, Y. Wang, E. A. Fitzgerald, and C. Seng Tan, "Suppression of interfacial voids formation during silane (SiH4)-based silicon oxide bonding with a thin silicon nitride capping layer," J. Appl. Phys. **123**(1), 015302 (2018).
42. B. Son, Y. Lin, K. H. Lee, Y. Wang, S. Wu, and C. S. Tan, "High speed and ultra-low dark current Ge vertical pin photodetectors on an oxygen-annealed Ge-on-insulator platform with GeO x surface passivation," Opt. Express **28**(16), 23978–23990 (2020).

155.69.250.71 {ts '2020-11-02 20:08:59'}